QCD sum rules at low temperature

C. Adami, T. Hatsuda, and I. Zahed

Physics Department, State University of New York at Stony Brook, Stony Brook, New York, 11794

(Received 30 November 1989; revised manuscript received 7 May 1990)

We discuss finite-temperature QCD sum rules at low temperatures, including perturbative as well as nonperturbative thermal corrections. The electric and magnetic condensates of the thermalized QCD state are extracted from present lattice calculations of the energy density and pressure. Alternative parametrizations based on instanton calculations and string behavior at finite temperature are also discussed. Throughout, a particular emphasis is put on the nature and size of the temperature corrections. In the 1^- channel the temperature behavior of the ρ parameters are investigated. In the range of applicability of the sum-rule procedure, the ρ parameters are found to vary slowly with temperature.

I. INTRODUCTION

Recently there has been increasing theoretical interest in hadronic matter under extreme conditions of temperature and density following the recent experiments at CERN SPS using ultrarelativistic heavy-ion collisions.[1] It is generally believed that at high temperature or density bulk hadronic matter undergoes a phase transition to a plasma of quarks and gluons. This idea is supported by lattice Monte Carlo calculations.[2,3]

Monte Carlo simulations provide a powerful tool for investigating the nonperturbative character of QCD in the vacuum and in the presence of matter. However, the Euclidean formulation of the lattice calculations makes it difficult to analyze real-time correlation functions at finite temperature. Moreover, the analysis of QCD at finite density on the lattice has so far proved difficult.

A few years ago, Bochkarev and Shaposhnikov outlined an extension of the QCD sum rule to finite temperature and densities.[4] Using a variant of the QCD sum rules they investigated the dependence of the resonance mass and threshold parameters on the temperature in the vector channel. Their results show a rapid change in the resonance spectrum at about 150 MeV which they identified with the expected QCD phase transition. This transition was, however, criticized recently by Dosch and Narison,[5] who argue that it follows from an inappropriate use of the stability criterion. A similar concern has been raised by Furnstahl, Lee and one of us,[6] who have also extended the analysis to charmonium.

In this paper, we would like to address the problem of finite- (low-) temperature QCD sum rules with a special concern on the temperature dependence in the Wilson coefficients and vacuum condensates, a point so far (largely) ignored. In particular, we would like to investigate the changes in the mass and threshold parameters using input condensates that account for the general behavior of the thermalized QCD state, emphasizing throughout the role of temperature in the asymptotic expansion. Specifically, we calculate *all* temperature corrections to the Wilson coefficients of those operators that are retained in the operator-product expansion

(OPE) (to zeroth order in the quark-gluon coupling) and assess their size and relevance as compared to the temperature-dependent condensates. For the vacuum parameters, we will consider three alternatives. First, we will extract (in Minkowski space) the electric and magnetic condensates from the lattice calculations of the bulk energy and pressure at finite temperature (model I). Since the lattice results are still in a qualitative stage, we will consider a second parametrization of the vacuum parameters as implied by the finite-temperature instanton results of Nowak, Verbaarschot, and one of us[7,8] (model II). Finally, since instantons are not sufficient to trigger the correct string tension at zero temperature, we will present (qualitative) arguments for a third alternative based on the finite-temperature dependence of the string tension in the strong-coupling limit (model III). Our results show that the QCD sum-rule calculations become unreliable near T_c. Our analysis will be restricted to the case of zero chemical potential. The effects of density on the resonance spectrum will be discussed elsewhere.

II. THE METHOD

At finite temperature the relevant correlator is the thermal average of the retarded propagator (see, e.g., Refs. 9 and 10):

$$G_{\mu\nu}^R(q_0,\mathbf{q}) = i \int d^4x \, e^{iq\cdot x}\theta(x_0)\langle\langle 0|[J_\mu(x),J_\nu(0)]|0\rangle\rangle \,,$$

$$(2.1)$$

where J_μ is a pertinent QCD current. In the ρ channel we will use (unregularized)

$$J_\mu(x) = \tfrac{1}{2}[\bar{u}(x)\gamma_\mu u(x) - \bar{d}(x)\gamma_\mu d(x)] \,. \qquad (2.2)$$

To distinguish the long- and short-wavelength contributions to (2.1) we will make use of the OPE for the commutator. Details of the procedure can be found in the original paper by Wilson.[11] At short distances $(x \to 0)$, the contributions to (2.1) can be organized in an asymptotic series using local and Becchi-Rouet-Stora-Tyutin-(BRST-)invariant bilinears of increasing dimensionality (normal ordering understood):

$$[J(x), J(0)] = \mathcal{C}_1(x)\mathbf{1} + \mathcal{C}_{\bar{q}q}(x)m\bar{q}q + \mathcal{C}_{E^2}(x)\mathbf{E}^2$$
$$+ \mathcal{C}_{B^2}(x)\mathbf{B}^2 + \cdots , \qquad (2.3)$$

where $q(x)$ is the quark field operator and $\mathbf{E}$ and $\mathbf{B}$ the electric and magnetic gluon fields. The short-distance singularities are lumped in the Wilson coefficients $\mathcal{C}$ and can be evaluated in perturbation theory.[12] Since the operators in (2.3) have various dimensions, the Fourier transform of the Wilson coefficients involves increasing powers of $1/Q^2$ reflecting the dominant contribution of operators of the lowest dimensions at short distances.

The true (nonperturbative) vacuum is believed to support Lorentz-invariant quark and gluon condensates. Conventional sum rules suggest[13]

$$\langle \bar{q}q \rangle = (-250 \text{ MeV})^3$$

and

$$\langle (2\alpha_s/\pi)(B^2 - E^2) \rangle = (330 \pm 20 \text{ MeV})^4 .$$

At zero temperature normal ordering is enforced in the perturbative vacuum. If this ordering is kept at finite temperature, the Wilson coefficients remain T independent while the composite operators acquire thermal perturbative *and* nonperturbative effects. To sort out the perturbative contribution from the composite operators a reordering in the heat bath is needed. This is achieved by formulating the finite temperature problem using thermo-field dynamics where the T vacuum is defined analogously to the zero-temperature vacuum. In this spirit, normal ordering at finite temperature will be enforced in the T vacuum following the doubling of the field variables.[14] As a result, the Wilson coefficients in (2.3) acquire an additional temperature dependence so that the thermal averages of the composite operators no longer involve thermal perturbative effects. In a way, this corresponds to a nontrivial rearrangement of the OPE around the blackbody spectrum.[15]

Throughout, we will enforce the above considerations by using the background-field formalism at finite temperature to evaluate the Wilson coefficients. At zero temperature, this method is equivalent to using the OPE. At finite temperature the generic form of the Wilson coefficients is $[Q = (iq_0; \mathbf{q} = 0)]$

$$\mathcal{C}_{E^2} = \mathcal{C}_{E^2}^{(1)} \frac{1}{Q^2} + \mathcal{C}_{E^2}^{(2)} \frac{T^2}{Q^4} + \mathcal{C}_{E^2}^{(3)} \frac{T^4}{Q^6} + \cdots . \qquad (2.4)$$

At very low temperatures $(T \ll T_c)$ the temperature dependence in the Wilson coefficients and the vacuum condensates is small when the external energy is about the resonance mass. The effects of higher condensates $(d > 6)$ can be ignored just as in the zero-temperature case. For temperatures of the order of $T \sim T_c \sim \sqrt{E}$ the contributions from higher-dimensional operators become comparable to the temperature corrections. For consistency, an expansion in operators of higher dimensions requires a commensurate expansion in T. Hence, we will limit the discussion to low temperatures $(0 < T < T_c)$ and keep only terms of order Q^{-6} in the expansion.

The retarded commutator (2.1) is analytic in the upper

half plane and obeys the dispersion relation (modulo subtractions)

$$\text{Re}G_{\mu\nu}^R(Q_2) = \frac{Q^2}{\pi} \int_0^\infty \frac{\text{Im}G_{\mu\nu}^R(s)}{s(s+Q^2)} ds . \qquad (2.5)$$

At finite temperature, $G_{\mu\nu}^R$ is characterized by a transverse (G_T) and a longitudinal (G_L) form factor:[16]

$$G_{ij}^R = \left[\delta_{ij} - \frac{Q_i Q_j}{\mathbf{Q}^2} \right] G_T + \frac{Q_i Q_j}{\mathbf{Q}^2} Q_0^2 G_L , \qquad (2.6)$$

$$G_{00}^R = \mathbf{Q}^2 G_L . \qquad (2.7)$$

In the resonance rest frame the two form factors are related to each other: $G_T \to Q^2 G_L$ with $\mathbf{Q} \to 0$. Hence, it is sufficient to study the longitudinal form factor. From now on the source will be taken at rest in the heat bath.

The imaginary part in (2.5) [right-hand side (RHS)] involves poles and cuts and cannot be evaluated in perturbation theory. We parametrize the RHS in the ρ channel using a pole mass at m_ρ with a strength f_ρ, a threshold energy S_0, and a scattering term S_ρ for soft thermal dissociations (mainly through pions) at $s = 0$. Specifically,

$$\text{Im}G_L(s) = f_\rho m_\rho^2 \pi \delta(s - m_\rho^2)$$
$$+ \theta(s - S_0) \frac{1}{8\pi} \tanh \left[\frac{\sqrt{s}}{4T} \right] + S_\rho \pi \delta(s) . \qquad (2.8)$$

Following the usual sum-rule procedure we have used the temperature dependence of the imaginary part of the thermalized vacuum for an optimal parametrization of the threshold part.

The OPE expansion yields perturbative information on the real part of Eq. (2.1) [LHS of (2.5)] in the deep Euclidean region $(Q^2 \to \infty)$. To evaluate the real part of the retarded propagator we can use thermo-field dynamics for the Feynman propagator and then analytically continue it to the Euclidean axis. Equivalently, we can just calculate the real part of the Matsubara propagator for $q^0 = \omega_n = i2\pi nT$ and then analytically continue it to the full Euclidean axis. The leading perturbative contribution to the Matsubara propagator is shown in Fig. 1(a). For simplicity, we have not included radiative corrections to $\mathcal{C}_1$. At $T = 0$, this contribution is small (about 5%). We expect these effects to be even smaller at finite temperature, as the coupling constant runs down. The calculation of $O(\alpha_s)$ corrections at finite temperature is prohibitive. We hope, however, to explore this point in a further investigation.

Figures 1(b)–1(e) show the leading nonperturbative contributions as implied by the OPE. As in the zero-temperature case the contribution in Fig. 1(b) vanishes in the chiral limit. As for Fig. 1(d), its contribution turns out to be infrared divergent at finite temperature in the chiral limit. We shall comment on this below. The contributions of the electric and magnetic condensates of the type shown in Figs. 1(c) and 1(d) are in general different since in the heat bath the vacuum is O(3) rather than O(4) invariant. As already pointed out higher-dimensional operators and higher powers of T are suppressed by
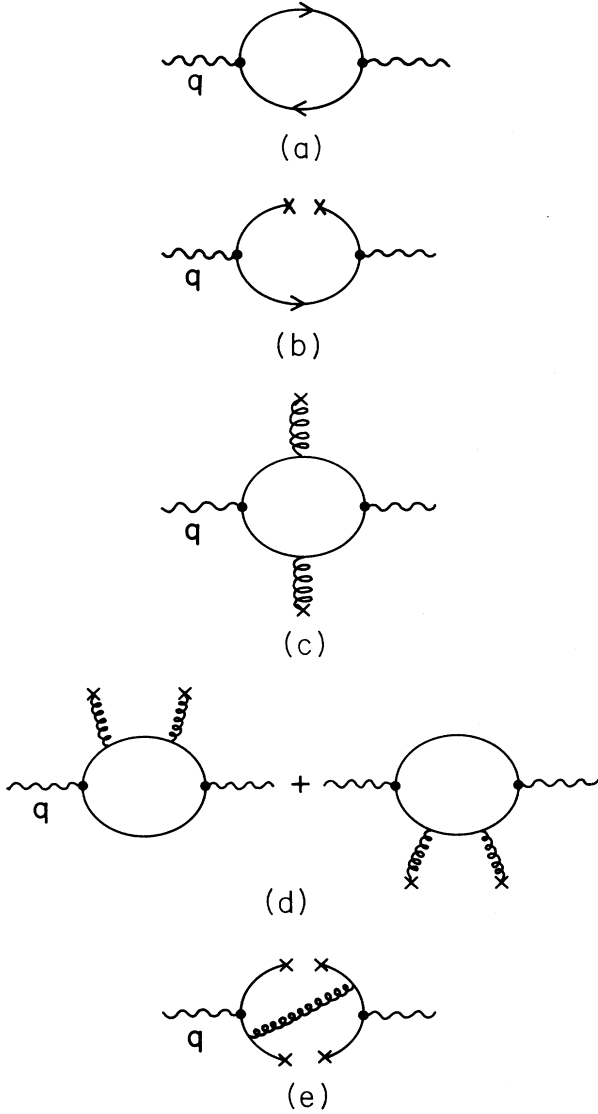
FIG. 1. (a) Leading perturbative contribution to the OPE: coefficient $\mathcal{C}_1$; (b) contribution of the quark condensate $\mathcal{C}_{\bar{q}q}$; (c) contribution of gluonic operators: coefficients $\mathcal{C}^a_{E^2}$ and $\mathcal{C}^a_{B^2}$; (d) coefficients $\mathcal{C}^b_{E^2}$ and $C^b_{B^2}$; (e) coefficient $\mathcal{C}_{(\bar{q}q)^2}$.

powers of the external momentum Q^2. In the real-time formalism the calculation is similar to the zero-temperature case except for the introduction of ghost fields to take care of the pinch singularities. This approach is described in Appendix A. The results for the Wilson coefficients in both the real and imaginary time approaches agree and read

$$\mathcal{C}_1 = -\frac{1}{8\pi^2}\ln Q^2 + \frac{7}{15}\pi^2\frac{T^4}{Q^4} - \frac{248}{63}\pi^4\frac{T^6}{Q^6} , \qquad (2.9)$$

$$\mathcal{C}^a_{E^2} = -\frac{\alpha_s}{6\pi}\frac{1}{Q^4} + \frac{2}{9}\alpha_s\pi\frac{T^2}{Q^6} , \qquad (2.10)$$

$$\mathcal{C}^b_{E^2} = -\frac{8\alpha_s}{9\pi}\frac{1}{Q^4}\left[1 - \ln\frac{Q^2}{\mu^2} - 4\pi^2\frac{T^2}{Q^2}\right] , \qquad (2.11)$$

$$\mathcal{C}^a_{B^2} = -\frac{4}{9}\alpha_s\pi\frac{T^2}{Q^6} , \qquad (2.12)$$

$$\mathcal{C}^b_{B^2} = -\frac{8\alpha_s}{9\pi}\frac{1}{Q^4}\left[1 - \ln\frac{Q^2}{\mu^2} - 4\pi^2\frac{T^2}{Q^2}\right] , \qquad (2.13)$$

$$\mathcal{C}_{(\bar{q}q)^2} = -\frac{112}{81}\pi\alpha_s , \qquad (2.14)$$

where only terms of order Q^{-6} have been retained. The unexpanded expressions are quoted in Appendix B. To check the reliability of the temperature expansion we have performed calculations with both the expanded and the unexpanded (resummed) Wilson coefficients.

We have ignored $d=6$ gluon operators such as $\mathbf{E}\cdot(\mathbf{E}\times\mathbf{B})\cdots$. At zero temperature, they combine to the Lorentz-invariant form $f^{abc}F^aF^bF^c$. The latter is found to give zero contribution to correlations in the quark bilinears.[17,18] This is no longer true at finite temperature due to the lack of manifest Lorentz invariance in the heat bath. However, since these operators are suppressed in the range $0 < T < T_c$ as compared to the lower-dimensional operators, we have ignored them.

The Wilson coefficients for $\mathbf{E}^2$ and $\mathbf{B}^2$ are infrared divergent. At zero temperature, however, we have $\langle \mathbf{E}^2 \rangle = -\langle \mathbf{B}^2 \rangle$ so that the infrared divergence drops from the Lorentz- and gauge-invariant combinations in the chiral limit. This is no longer true at finite temperature. The infrared divergence is due to Fig. 1(d) when the quark line between the gluon insertions becomes soft. At zero temperature and for nonvanishing current masses, this soft contribution is lumped into $m\bar{q}q$ using the equations of motion.[19] Since the argument holds at the operator level, it will be understood throughout.

As in the zero-temperature case one hopes to match the perturbative calculation (LHS) with the nonperturbative parametrization[20] (RHS) using a Borel transformation with a Borel parameter M^2 around the resonance region. Equating the Borel transform of the RHS with the Borel transform of the LHS, we obtain the sum-rule result

$$8\pi^2 f_\rho\frac{m_\rho^2}{M^2}e^{-m_\rho^2/M^2} = R(M^2,T^2) , \qquad (2.15)$$

where

$$R(M^2,T^2) = 1 - e^{-S_0/M^2} + 8\pi^2\left[\frac{1}{6}\frac{T^2}{M^2} - \frac{S_\rho(T)}{M^2}\right] - 8\int_0^{S_0/4}\frac{dx^2}{M^2}n_F(x/T)\mathcal{A}(x)$$

$$-\frac{1}{3}\frac{\pi^2}{M^4}\left\langle\!\left\langle\frac{\alpha_s}{\pi}4\mathbf{E}^2\right\rangle\!\right\rangle - \frac{8}{9}\pi^4\frac{T^2}{M^6}\left[2\left\langle\!\left\langle\frac{\alpha_s}{\pi}\mathbf{B}^2\right\rangle\!\right\rangle - \left\langle\!\left\langle\frac{\alpha_s}{\pi}\mathbf{E}^2\right\rangle\!\right\rangle\right] - \frac{448}{81}\pi^3\alpha_s\frac{\langle\!\langle\bar{q}q\rangle\!\rangle^2}{M^6} \qquad (2.16)$$

with $n_F(x/T) = (1 + e^{x/T})^{-1}$ and

$$\mathcal{A}(x) = 1 - 4\frac{x^2}{M^2} + 8\frac{x^4}{M^4} \ . \tag{2.17}$$

Note that the perturbative temperature corrections to $\mathcal{C}_1$ given by (2.9) cancel most of the temperature dependence in the parametrized threshold part given by (2.8). The left over is the fourth term in (2.16). This cancellation follows from the duality of the quark spectrum and the hadron spectrum at high momentum. As a result, the temperature corrections do not overwhelm the perturbative contribution at low temperatures.

III. VACUUM PARAMETERS

Since at present there is no final consensus on the vacuum condensates at finite temperature, we will investigate three different but complementary cases. First we will extract the condensates from present measurements of the bulk properties of finite temperature QCD on the lattice. We shall refer to this parametrization henceforth as model I.

The equilibrium energy density and pressure of QCD matter on the lattice is evaluated using

$$\mathcal{E} = \alpha \langle\langle E^2 + B^2 \rangle\rangle_{\text{lattice}} + \gamma \langle\langle B^2 - E^2 \rangle\rangle_{\text{lattice}} \ ,$$
$$\mathcal{P} = \frac{\alpha}{3} \langle\langle E^2 + B^2 \rangle\rangle_{\text{lattice}} - \gamma \langle\langle B^2 - E^2 \rangle\rangle_{\text{lattice}} \ , \tag{3.1}$$

where $\langle\langle E^2 \rangle\rangle$ and $\langle\langle B^2 \rangle\rangle$ are the continuum limit of the timelike and spacelike plaquette actions (Minkowski notation). Using gluons only ($N_c = 3$), the coefficients in (3.1) are given by[21]

$$\alpha = 0.5 - 0.083\,39g^2 + O(g^4) \ ,$$
$$\gamma = 0.0 - 0.017\,42g^2 + O(g^4) \ . \tag{3.2}$$

Note that (3.2) yields the correct trace anomaly on the lattice. These condensates contain both perturbative and nonperturbative contributions. On the lattice the subtraction can be performed as follows:

$$\langle\langle E^2 \rangle\rangle = (\langle\langle E^2 \rangle\rangle - \langle\langle E^2 \rangle\rangle_0)_{\text{lattice}} - \langle\langle E^2 \rangle\rangle_* + \langle E^2 \rangle \ ,$$
$$\langle\langle B^2 \rangle\rangle = (\langle\langle B^2 \rangle\rangle - \langle\langle B^2 \rangle\rangle_0)_{\text{lattice}} - \langle\langle B^2 \rangle\rangle_* + \langle B^2 \rangle \ . \tag{3.3}$$

First, the zero-temperature data on the lattice are subtracted from the raw condensates at finite temperature. The result contains finite-temperature perturbative $\langle\langle \ \rangle\rangle_*$ and nonperturbative contributions. We have subtracted the former by using the asymptotic form of the energy density at high temperature on the lattice with $\mathcal{P}_* = \mathcal{E}_*/3$. Finally we have added the zero-temperature vacuum condensate as implied by lattice estimates and sum rules.

Figure 2 shows the behavior of the vacuum condensates using the lattice results for the energy density and pressure of the Columbia group.[22] The calculations have been carried out on a $16^3 \times 4$ lattice. For $\mathcal{E}_*$ we take the value of the energy density at the highest temperature of the data set. Below T_c ($\beta_c = 5.6925$), $\mathcal{E}$ and $\mathcal{P}$ are consistent with zero. We extrapolate this behavior to zero
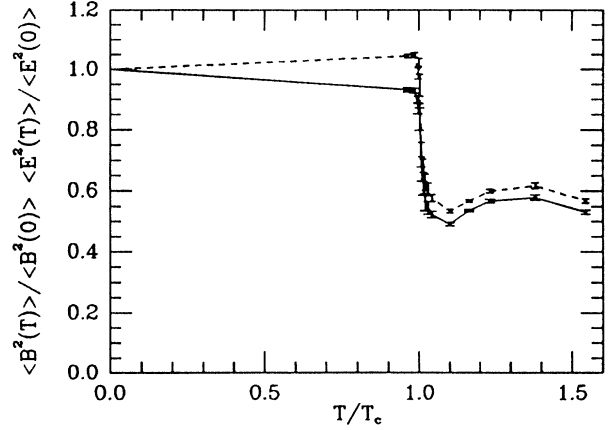
FIG. 2. Vacuum condensates from lattice results (model I). The full curve shows the behavior of $\langle\langle B^2 \rangle\rangle$ normalized to its zero-temperature value, the dashed curve represents the normalized $\langle\langle E^2 \rangle\rangle$.

temperature, which gives almost constant values of the condensates below T_c. The figure indicates that the condensates do not vanish above T_c. In the range $T_c < T < 2T_c$ we see that $\langle\langle B^2 \rangle\rangle \sim -\langle\langle E^2 \rangle\rangle$. The condensates have dropped by about 50%. This is consistent with recent lattice estimates of the electric and magnetic condensates for SU(2) at high temperature.[23] The nonvanishing of the gluon condensates well above T_c stems from the fact that the pressure $\mathcal{P}$ lags behind the energy density $\mathcal{E}/3$ in approaching the Stefan-Boltzmann limit.

At present, large scale SU(3) simulations with light quarks are not available. As an example we have taken a 4-flavor simulation by Kogut and Sinclair[24] (similar results have been obtained by Karsch et al.[25]). Since these simulations are performed in a narrow temperature interval very close to T_c, a global dependence of the quark condensate on temperature cannot be extracted. In order to achieve this, additional simulations on lattices with larger temporal extent (lower temperature) are required. We have used the 4-flavor simulation by Grady, Sinclair, and Kogut[26] on a symmetric (8×8^3) lattice to tentatively extract a temperature profile for the quark condensate. To set the scale at $T = 0$ we have used their calculation of the ρ mass, thereby eliminating the lattice spacing, and fixing the normalization. For $T \neq 0$ we have enforced $T_c = 140$ MeV, which is slightly larger than the value estimated in Ref. 26. This sets the normalization of the lattice results around T_c. Figure 3 shows the behavior of the quark condensate (normalized to its zero-temperature value) constructed by interpolating these two lattice calculations. The lattice results of Kogut and Sinclair indicate a first-order transition. Recent calculations for the interesting case of two light flavors on an 8×12^3 lattice by Gottlieb et al.[27] seem to suggest a much weaker transition, although an extrapolation to zero temperature is not possible.

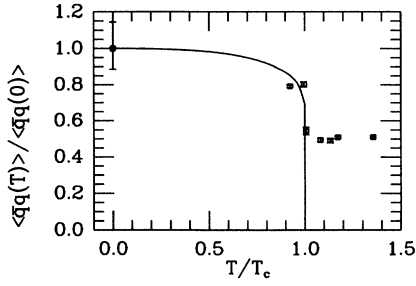A second albeit model-dependent choice for the vacuum parameters stems from the instantons description of

FIG. 3. (a) $\langle\langle \bar{q}q \rangle\rangle$ condensate in model I (points from Ref. 24 and Ref. 26). The solid curve is our interpretation of these points. Since the absolute values suggested by the lattice calculation are unreliable we have normalized at zero temperature.

the QCD vacuum. Assuming that the QCD partition function is dominated by instanton and anti-instanton fluctuations yields a reasonable description of the QCD ground state. Instantons and anti-instantons stabilize in the vacuum in a disordered quantum state similar to a quantum liquid. In the latter, chiral symmetry is spontaneously broken following the delocalization of the fermion zero modes. With increasing temperature the instantons and anti-instantons are found to boil off the vacuum restoring chiral symmetry. The behavior of the instanton density $n(T)$ and the fermion condensate at finite temperature have been investigated by Nowak, Verbaarschot, and one of us.[7,8] Their results (for two flavors) are shown in Figs. 4(a)–4(b). Since the instanton solutions
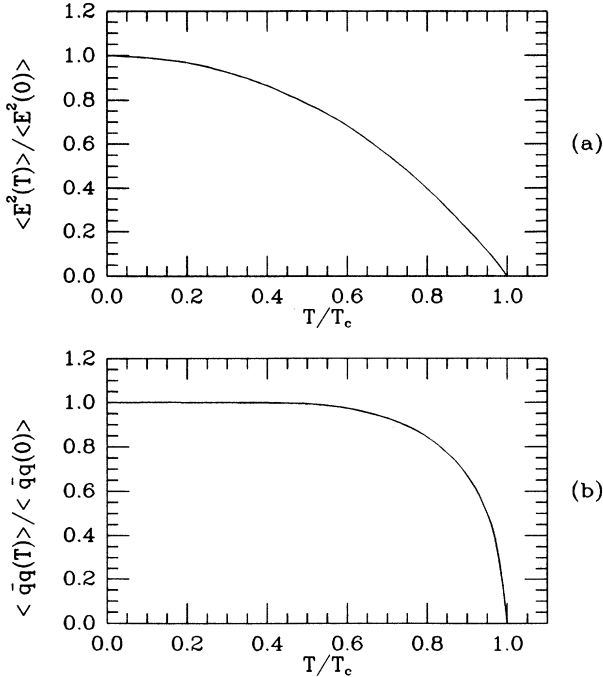
are self-dual we have (in Minkowski space)

$$\langle\langle B^2 \rangle\rangle = -\langle\langle E^2 \rangle\rangle = n(T)/4 \ .$$

At T_c both the electric and magnetic condensates vanish. This parametrization will be referred to as model II. The instanton calculation underestimates the string tension by about 50% at zero temperature.

A third *possible* parametrization of the vacuum condensates can be inferred *partly* from strong-coupling arguments (model III). Overall, lattice QCD calculations suggest a disordering of the timelike Wilson loop and a vanishing of the fermion condensate at some critical temperature T_c. The disordering of the timelike Wilson loop leads to a vanishing of the string tension $\sigma(T)$. This behavior is supported by calculations using string models. Using a bosonic string in $d = \infty$ dimensions Alvarez and Pisarski[28] have shown that the string tension scales as follows:

$$\sigma(T) = \sigma(0)\left[1 - \frac{T^2}{T_c^2}\right]^{1/2} \ . \tag{3.4}$$

Dimensional arguments suggest that $\langle\langle E^2 \rangle\rangle \sim -\sigma^2$. This parametrization is justified in the strong-coupling limit. Since spacelike Wilson loops display an area-law behavior above the critical temperature,[29] we expect $\langle\langle B^2 \rangle\rangle \sim \langle B^2 \rangle$. For consistency, we will use $\langle\langle \bar{q}q \rangle\rangle \sim -\sigma^{3/2}$ as suggested by dimensional arguments. This scaling is only suggestive, since the model does not allow for a direct calculation of the quark condensate.
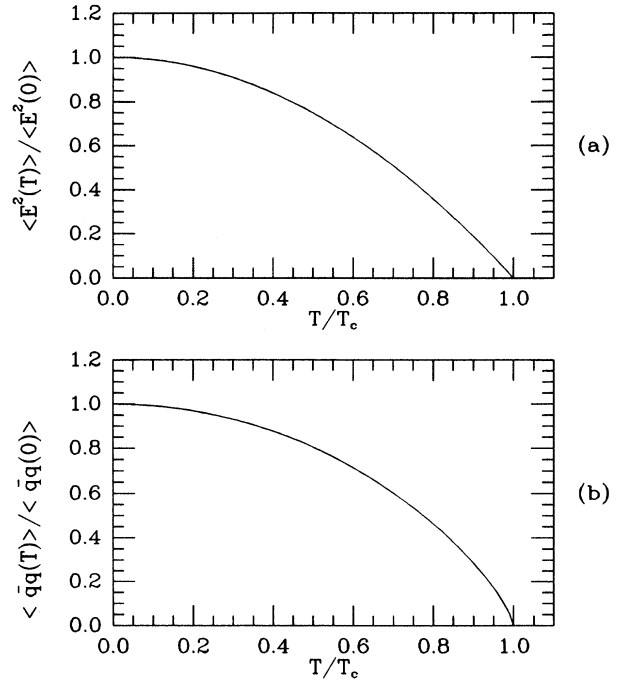

FIG. 4. Temperature dependence of the condensates from the instanton liquid model (model II) (from Ref. 8). (a) $\langle\langle E^2 \rangle\rangle$ and $\langle\langle B^2 \rangle\rangle$ condensate; (b) $\langle\langle \bar{q}q \rangle\rangle$ condensate.

FIG. 5. Temperature dependence of the condensates as implied by a string model (model III). (a) $\langle\langle E^2 \rangle\rangle$ condensate; (b) $\langle\langle \bar{q}q \rangle\rangle$ condensate. The magnetic condensate is kept temperature independent.
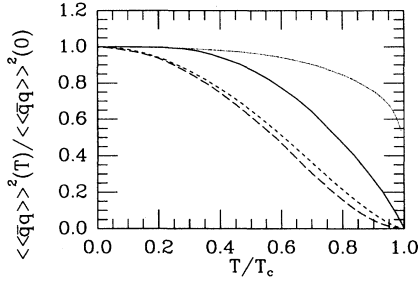
FIG. 6. Temperature dependence of the *square* of the condensates. The full line is taken from Ref. 4 and serves for comparison. The dotted line shows the profile as used in model (I). Model (II): long dashed line; model (III): short-dashed line.

However, this scaling is consistent with models I and II. The temperature dependence of the condensates in this parametrization is shown in Figs. 5(a)–5(b).

In order to compare these parametrizations of the quark condensate with the one used by Bochkarev and Shaposhnikov,[4] we plot the *square* of our condensates against T/T_c (this is the quantity that enters in the sum rule) and compare this behavior with the model assumption of Ref. 4. As is apparent from Fig. 6, the choice of Ref. 4 lies in between our choices.

IV. THE RESULTS

In order to extract the ρ parameters form the sum rule (2.15), we minimize the difference squared $(\text{LHS}-\text{RHS})^2$, which is a function of the Borel parameter M^2, the ρ mass m_ρ, the ρ strength f_ρ, the threshold energy S_0, and S_ρ in a given range of the Borel parameter (window). In order to have a reliable estimate for the ρ-meson parameters we follow SVZ in choosing the window in such a way that the nonperturbative contributions to the sum rule do not exceed 30% at small M^2 (dominance of the perturbative contribution). Likewise, we fix the right boundary (large M^2) by requiring that the contribution of the continuum remains smaller than 30% of the contribution of the resonance (resonance dominance). We then adjust the parameters m_ρ, f_ρ, and S_0 in such a way that $(\text{LHS}-\text{RHS})^2$ is minimal for *all* M^2 inside the Borel window. This is done, for the resummed version of the sum rules, for temperatures $0 < T/T_c < 1$ using an optimization routine. The results of this procedure are the full lines in Figs. 7–10. For the sum rules that rely on expanded Wilson coefficients this method is used for $0 < T/T_c < 0.6$ (dashed lines in Figs. 7–10). For $T/T_c > 0.6$ we have adjusted the parameters for various points between $0.6 < T/T_c < 0.95$ to show the qualitative behavior of the mass, the threshold, and the coupling. These points are marked by squares in the figures.

Typically, the width of the window is $\Delta M^2 \sim 1$ GeV^2 at $T = 0$ to cover the resonance and some of the continuum and decreases only slightly at higher temperatures. Around T_c the window is only a fraction of that value, however, since power corrections and continuum contributions are large.
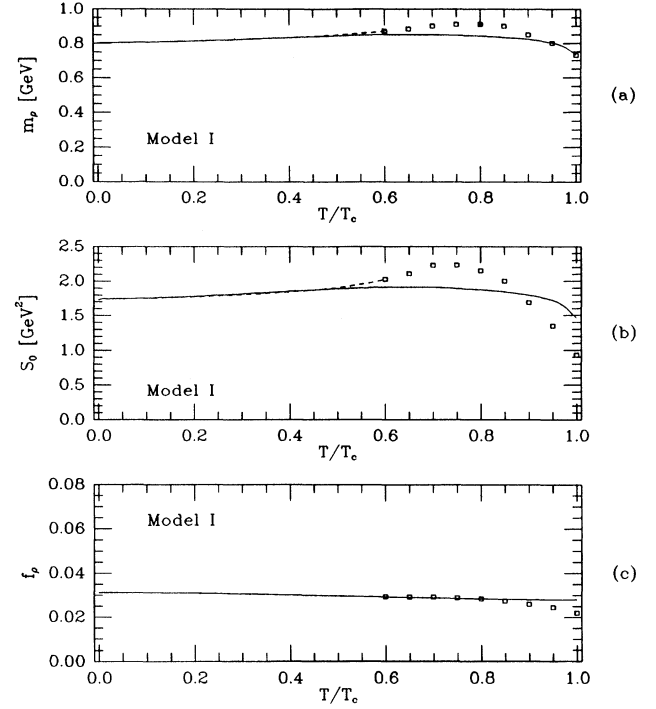
FIG. 7. ρ-meson parameters from model I. (a) ρ-meson mass; (b) continuum threshold S_0; (c) resonance strength f_ρ. The dashed lines and squares are calculated using expanded coefficients, the full lines using the resummed coefficients.
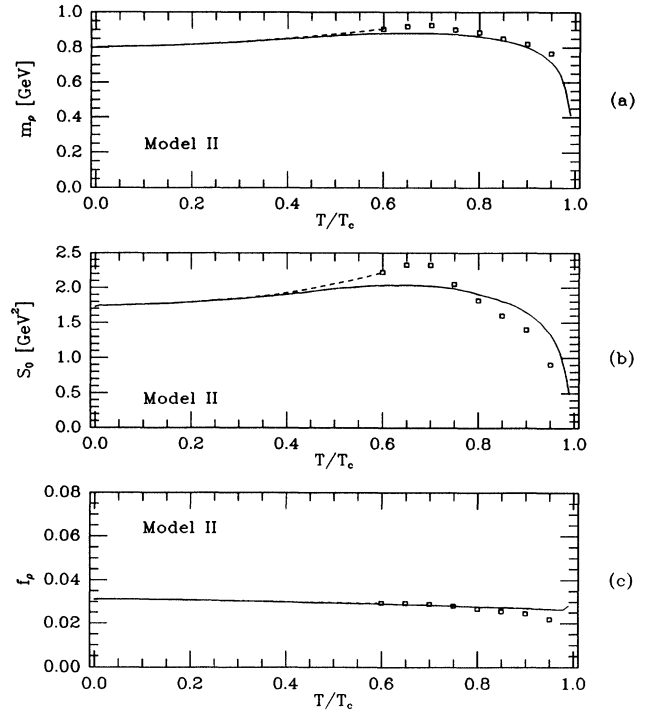
FIG. 8. ρ-meson parameters from model II. (a) ρ-meson mass; (b) continuum threshold S_0; (c) resonance strength f_ρ. Notation as in Fig. 7.
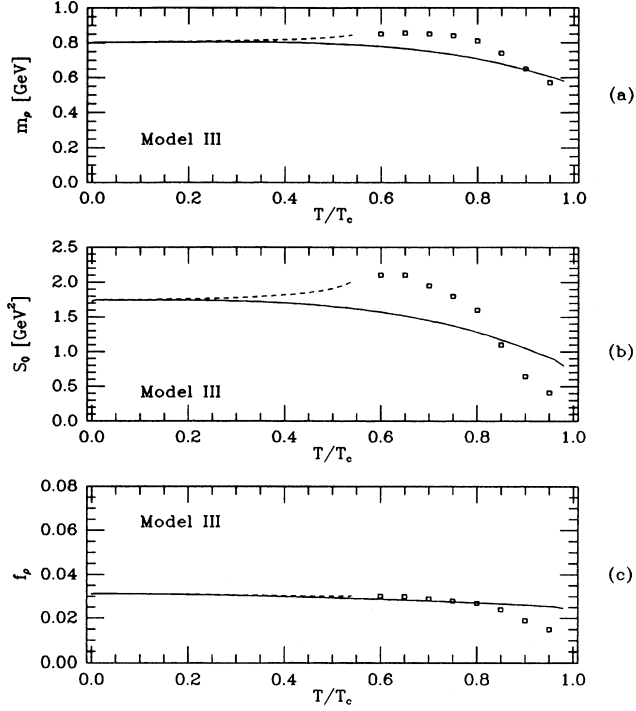
FIG. 9. ρ-meson parameters from model III. (a) ρ-meson mass; (b) continuum threshold S_0; (c) resonance strength f_ρ. Notation as in Fig. 7.

Throughout, we use

$$S_\rho = \frac{1}{24\pi^2} \int_0^2 dx^2 2n_B(x/2T) = \frac{1}{9}T^2 , \qquad (4.1)$$

where $n_B(x)$ is the bosonic distribution function. This is expected on general grounds if the medium consists predominantly of free massless pions (see, e.g., Ref. 4). The latter situation seems to prevail below the deconfining transition. As a check we have performed the same calculation with a different $S_\rho(T)$, namely one that is expected above the deconfining transition (medium of free quarks). In this case $S_\rho(T) = \frac{1}{6}T^2$. Changes of that order do not affect considerably the present calculation. At $T = 0$ we overestimate the experimental values of the ρ-meson parameters by about 5%:[30] $m_\rho = 805$ MeV, $f_\rho = 0.032$ and $S_0 = 1.75$ GeV^2. The strength of the resonance is related to the ρ coupling constant through

$$g_\rho^2 = \frac{1}{f_\rho} , \qquad (4.2)$$

such that we obtain

$$\frac{g_\rho^2}{4\pi} = 2.49 . \qquad (4.3)$$

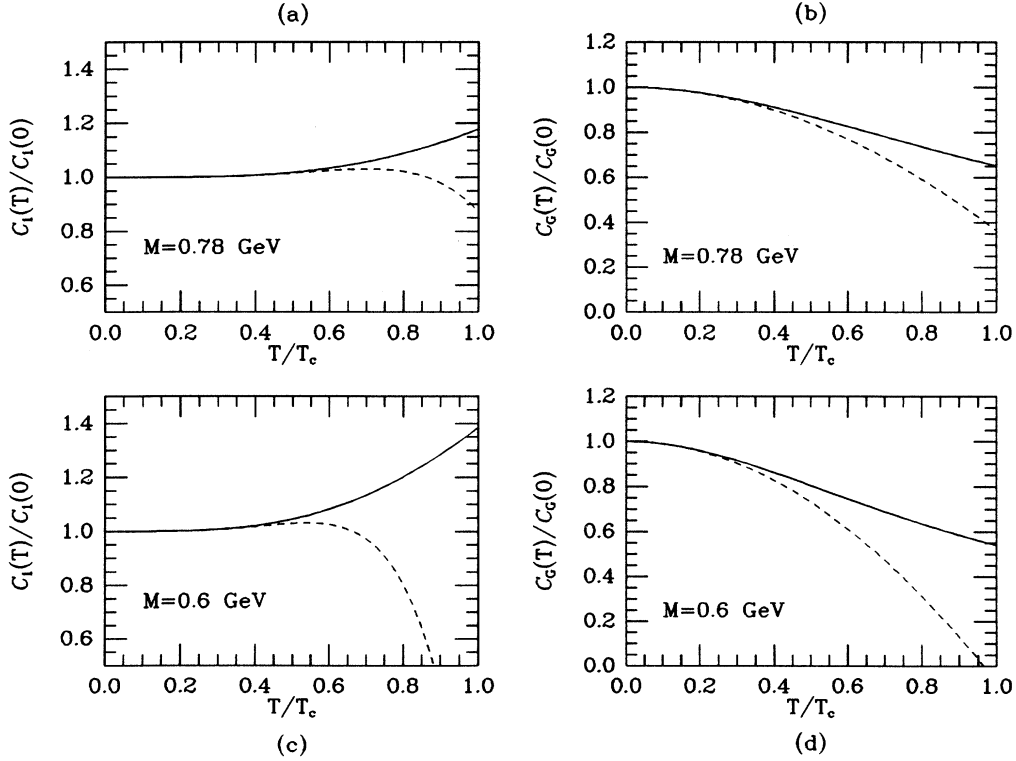This is also close to the experimental value[31]

FIG. 10. Temperature dependence of the Borel transformed Wilson coefficients for two typical values of the Borel mass. (a) $\mathcal{C}_1(T)/\mathcal{C}_1(0)$ at $M = 0.78$ GeV; (b) $\mathcal{C}_{G^2}(T)/\mathcal{C}_{G^2}(0)$ at $M = 0.78$ GeV; (c) $\mathcal{C}_1(T)/\mathcal{C}_1(0)$ at $M = 0.5$ GeV; (d) $\mathcal{C}_{G^2}(T)/\mathcal{C}_{G^2}(0)$ at $M = 0.5$ GeV.

TABLE I. Splitting of the contributions to the sum rule for the lattice model (model I). LHS: splitting into perturbative (vacuum) and nonperturbative contributions; RHS: splitting between excitations. The contributions to the LHS and to the RHS respectively are normalized in such a way that they sum up to 1 (up to rounding errors).

T/T_c		LHS			RHS	
	Vacuum	$\langle\langle G^2 \rangle\rangle$	$\langle\langle (\bar{q}q)^2 \rangle\rangle$	Reson.	Contin.	Dissoc.
0.0 (full)	1.023	0.098	−0.121	0.93	0.07	0.0
0.0 (expanded)	1.023	0.098	−0.121	0.93	0.07	0.0
0.6 (full)	1.009	0.070	−0.079	0.845	0.070	0.085
0.6 (expanded)	1.012	0.056	−0.068	0.845	0.074	0.081
0.7 (full)	1.007	0.067	−0.074	0.818	0.069	0.113
0.7 (expanded)	1.007	0.045	−0.052	0.832	0.067	0.101
0.8 (full)	1.006	0.066	−0.072	0.786	0.067	0.147
0.8 (expanded)	1.006	0.039	−0.046	0.801	0.071	0.129
0.9 (full)	1.004	0.069	−0.072	0.749	0.062	0.189
0.9 (expanded)	1.020	0.043	−0.063	0.755	0.053	0.193
0.95 (full)	1.001	0.073	−0.074	0.727	0.058	0.215
0.95 (expanded)	1.041	0.048	−0.089	0.751	−0.007	0.256

$$\left[\frac{g_\rho^2}{4\pi} \right]_{\text{expt}} = 2.36 \pm 0.18 \ . \tag{4.4}$$

Using the lattice condensates (model I) the behavior of the ρ mass is shown in Fig. 7(a), the behavior of the threshold energy S_0 is shown in Fig. 7(b) and the ρ-meson strength f_ρ in Fig. 7(c) for a range of temperatures below T_c. We have used $T_c = 140$ MeV and the lattice results for the condensates in Fig. 3. The dashed curves and square points correspond to the expanded Wilson coefficients in the OPE, whereas the full curves correspond to the unexpanded Wilson coefficients as discussed in Sec. II. Because of the fact that the quark condensate on the lattice does not show a marked change below T_c there is accordingly no change in the ρ-meson parameters. This is a feature of the first-order transition. For a second-order transition the change in the parameters would be much more pronounced. The difference between the resummed and the expanded version of the sum rule is due to the different Wilson coefficients. The resummed coefficients are slowly varying functions of T in the range of parameters used here as shown in Fig. 10 for two different values of the Borel-parameter (full

curves) in contrast with the expanded coefficients (dashed curves). The latter have a T behavior that is opposite to the quark condensate. This cancels the dropping of the quark condensate at intermediate values of T.

Figures 8(a)–8(c) and 9(a)–9(c) show the behavior of the ρ-meson parameters using the instanton calculation (model II) and the string model (model III), respectively. Overall the ρ parameters are rather insensitive to large variations in the temperature below T_c when using the expanded Wilson coefficients. The reliability of the temperature expansion can be measured by the deviation of the expanded results (dashed curves) from the unexpanded results (solid curves). This is to be contrasted with Ref. 4 where a rapid variation in the ρ parameters is found. Notice however that the comparison is at best suggestive since neither the T dependence in the Wilson coefficients nor the T^2/Q^2 expansion were considered. Above $T/T_c = 0.6$ we have monitored the relative contributions of the vacuum and the condensates to the LHS of the sum rule; and of the resonance, the continuum and the dissociations [scattering term, see Eq. (2.8)] to the RHS of the sum rule. These numbers are collected in Tables I–III, for the models considered. We have displayed the contributions for both the expanded and

TABLE II. Contributions to the sum rule for the instanton model (model II). Normalization as in Table I.

T/T_c		LHS			RHS	
	Vacuum	$\langle\langle G^2 \rangle\rangle$	$\langle\langle (\bar{q}q)^2 \rangle\rangle$	Reson.	Contin.	Dissoc.
0.0 (full)	1.023	0.098	−0.121	0.93	0.07	0.0
0.0 (expanded)	1.023	0.098	−0.121	0.93	0.07	0.0
0.6 (full)	1.023	0.042	−0.066	0.848	0.072	0.081
0.6 (expanded)	1.021	0.034	−0.055	0.853	0.071	0.076
0.7 (full)	1.026	0.033	−0.059	0.819	0.072	0.108
0.7 (expanded)	1.020	0.023	−0.043	0.832	0.071	0.097
0.8 (full)	1.030	0.025	−0.055	0.783	0.073	0.144
0.8 (expanded)	1.029	0.018	−0.047	0.768	0.093	0.139
0.9 (full)	1.035	0.017	−0.052	0.731	0.068	0.202
0.9 (expanded)	1.038	0.010	−0.048	0.726	0.063	0.211
0.95 (full)	1.041	0.013	−0.054	0.680	0.056	0.264
0.95 (expanded)	1.038	0.006	−0.044	0.690	0.024	0.287

TABLE III. Contributions to the sum rule for the string model (model III). Normalization as in Table I.

T/T_c	Vacuum	LHS $\langle\langle G^2 \rangle\rangle$	$\langle\langle (\bar{q}q)^2 \rangle\rangle$	RHS Reson.	Contin.	Dissoc.
0.0 (full)	1.023	0.098	−0.121	0.93	0.07	0.0
0.0 (expanded)	1.023	0.098	−0.121	0.93	0.07	0.0
0.6 (full)	1.011	0.061	−0.072	0.826	0.073	0.101
0.6 (expanded)	1.007	0.035	−0.042	0.856	0.061	0.084
0.7 (full)	1.011	0.052	−0.063	0.784	0.072	0.144
0.7 (expanded)	1.008	0.022	−0.030	0.817	0.070	0.113
0.8 (full)	1.013	0.039	−0.051	0.729	0.068	0.203
0.8 (expanded)	1.018	0.006	−0.024	0.766	0.070	0.164
0.9 (full)	1.017	0.016	−0.033	0.657	0.054	0.290
0.9 (expanded)	1.188	−0.130	−0.058	0.832	−0.329	0.497
0.95 (full)	1.023	−0.060	−0.017	0.612	0.039	0.349
0.95 (expanded)	0.573	0.384	0.044	−0.933	2.955	−1.022

the resummed version of the sum rules for comparison. As is apparent from these tables, the expanded version of the sum rule breaks down earlier, mainly due to the fact that in this version the temperature effects are power corrections.

We have also estimated the leptonic width Γ_e ($\rho \to e^+ e^-$) and the strong decay width Γ_π ($\rho \to \pi\pi$) assuming vector dominance.[32] More specifically

$$\Gamma_e = \frac{\frac{1}{3}\alpha^2 m_\rho}{g_\rho^2/4\pi} \, , \quad (4.5)$$

with $k_\pi = \sqrt{m_\rho^2/4 - m_\pi^2}$. Figure 11 shows the behavior of the relative (normalized to the zero-temperature value) electronic width versus T/T_c for the three models discussed above. The full curves correspond to the unexpanded Wilson coefficients and the dashed curves and square points to the expanded coefficients. Surprisingly, the leptonic width decreases with temperature, by up to 20% at $T/T_c = 0.8$ depending on the model used. On the contrary, in the region where the sum rule can be trusted, the hadronic width tends to increase, by up to 30% at $T/T_c = 0.8$ (Fig. 12). The latter is only suggestive since
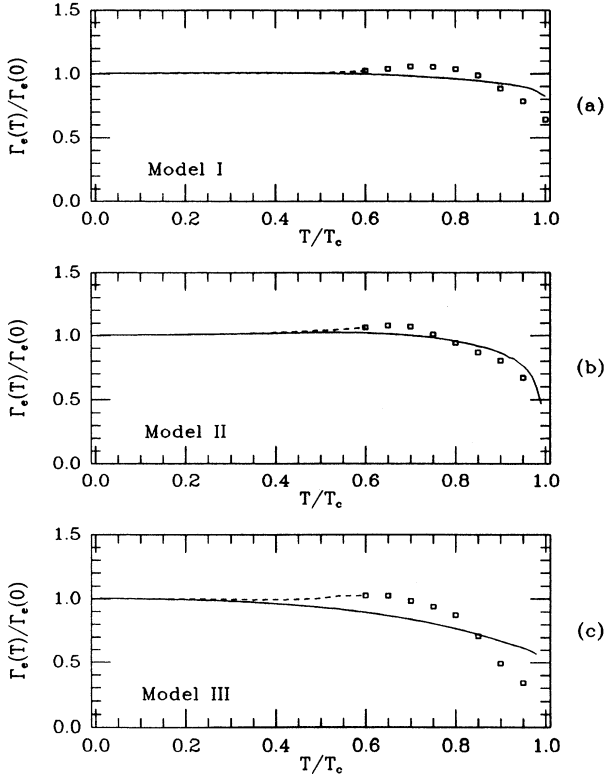

FIG. 11. Temperature dependence of the leptonic width $\Gamma_e(T)/\Gamma_e(0)$. Full line: resummed coefficients; dashed line and squares: expanded coefficients.
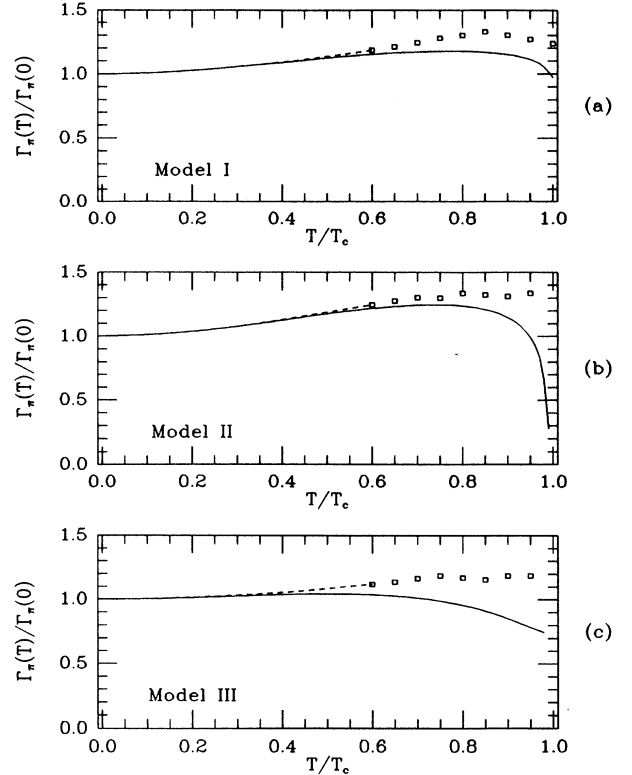
FIG. 12. Temperature dependence of the strong decay width $\Gamma_e(T)/\Gamma_e(0)$. Notation as in Fig. 11.

we have used a sharp resonance fit while parametrizing the pole term in the sum rules. This behavior of the strong width is consistent with one of the chiral mean-field analyses of Pisarski.[33]

V. CONCLUSION

We have analyzed the QCD sum rules below the phase transition in the ρ channel including perturbative and nonperturbative temperature corrections. In the range of temperatures considered we have argued for the relevance of a double expansion in both $1/Q^2$ and T^2/Q^2. We have used three different parametrizations for the vacuum parameters as motivated from the lattice calculations, the instanton liquid approach and the strong-coupling arguments. Overall, the ρ parameters are found to vary slowly with temperature in the range of temperatures where the separation between short- and long-wavelength fluctuations is reliable (a fraction of T_c). Around T_c the expansion breaks down as higher dimensional operators become important. To go beyond T_c requires a reassessment of the nonperturbative effects and a rearrangement in the vacuum structure. This issue is presently being investigated.[34]

APPENDIX A

In this appendix, we give an alternative derivation of the Wilson coefficients at finite temperature using the real-time formalism. In the real-time method, all the operators in the system are doubled to take into account the thermal effects. We also introduce an interaction of quarks with a background gauge field A_μ:

$$\mathcal{L}_{\text{int}} = g\bar{\Psi}\tau_3 T^a \gamma^\mu \Psi A_\mu^a ,\tag{A1}$$

where $\Psi = (\psi_1, \psi_2)$ is the doubled quark operator, τ_i are Pauli matrices acting on the doubled fields and $T^a = \lambda^a/2$. To remove the T-dependent pinch singularities (product of δ functions), it is necessary to couple A_μ^a to ψ_1 and ψ_2 with opposite signs. This is easily understood in thermo field dynamics: the tilde conjugate of A_μ^a is A_μ^a itself since the latter is real. The massless quark propagator in the real-time formalism reads

$$S_F = MDM ,\tag{A2}$$

with

$$M = \begin{bmatrix} \cos\theta & \sin\theta \\ -\sin\theta & \cos\theta \end{bmatrix} , \quad D = p_\mu \gamma^\mu \begin{bmatrix} \Delta & 0 \\ 0 & \Delta^* \end{bmatrix} ,\tag{A3}$$

where

$$\Delta = i(p^2 + i\epsilon)^{-1}$$

and

$$\cos^2\theta = (1 + e^{-|p_0|/T})^{-1} \equiv n_F(p_0) .$$

The Feynman diagram for the time-ordered correlation function

$$\Pi_{\mu\nu} = i \int d^4x\, e^{iqx} \langle\!\langle TJ_\mu(x)J_\nu(0) \rangle\!\rangle\tag{A4}$$

is easily written using the above propagator and the corresponding gluon propagator. The longitudinal part of the correlation function is obtained as $\Pi_L = -\Pi_\mu^\mu/3q_0^2$ when $\mathbf{q} = 0$. To calculate the Wilson coefficients of the gluonic operators, either the Fock-Schwinger (FS) gauge or the modified Fock-Schwinger (MFS) gauge is particularly useful

$$\text{FS:}\quad x_\mu A^\mu(t,\mathbf{x}) = 0 ,$$
$$\text{MFS:}\quad A^0(t,0) = 0 \quad\text{and}\quad x_i A^i(t,\mathbf{x}) = 0 .\tag{A5}$$

In the former case, $A_\mu(x)$ is expanded as

$$A_\mu(x) = \tfrac{1}{2}x^\nu G_{\nu\mu}(0) + \cdots ,$$

while

$$A_0(x) = x_i E_i(0) + \cdots$$

and

$$A_i(x) = \tfrac{1}{2}x^j G_{ji}(0) + \cdots$$

in the latter case. The LHS of the sum rule, i.e., the real part of the retarded correlation function in the asymptotic region $\text{Re}G_R(\omega)$ ($\omega = i\omega_I$ with $\omega_I \gg 1$) is equal to $\text{Re}G_F(\omega)$ for real ω.

The diagram in Fig. 1(c) in the FS gauge reads

$$\Pi_\mu^\mu(q) = \frac{i}{16} \int \frac{d^4p}{(2\pi)^4} \text{Tr}\{\gamma_\mu[S_F(p)\tau_3 \vec{V}_p^{\alpha\beta}S_F(p)]_{11}$$
$$\times \gamma_\mu[S_F(k)\vec{V}_k^{\lambda\rho}\tau_3 S_F(k)]_{11}\}$$
$$\times \langle\!\langle G_{\beta\alpha}^a G_{\rho\lambda}^a \rangle\!\rangle ,\tag{A6}$$

where Tr is the trace for spin indices, $k = p - q$, 11 denotes the 11-component of the matrix and $\vec{V}_p^{\alpha\beta} = \gamma^\alpha \vec{\partial}/\partial p_\beta$ appears while rewriting A_μ using the field strength.

The following Ward identity is useful to evaluate the product of propagators with momentum derivatives:

$$-i\frac{\partial S_F(p)}{\partial p_\mu} = S_F(p)\gamma_\mu\tau_3 S_F(p) + g_{\mu 0}\frac{\partial\theta}{\partial p_\mu}[\tau_2, S_F]_+ .\tag{A7}$$

It is easy to see that the second term in the RHS of (A7) can be rewritten as

$$2\pi i g_{\mu 0}\frac{\partial\theta}{\partial p_\mu}(p\cdot\gamma)\delta(p^2)M\tau_2 M .\tag{A8}$$

In the FS gauge, it can be shown by explicit calculation that this term does not contribute to the real part of the correlation function. This is more manifest in the MFS gauge where this term never appears since only the three-momentum derivative arises in the calculation. As a result (A6) reduces to a product of S_F without momentum derivatives, which is easy to evaluate using the following mass-derivative formula

$$(S_F \tau_3)_{11}^{n+1} = (p \cdot \gamma)^{n+1} \frac{1}{n!} \left[\frac{\partial}{\partial m^2} \right]^n \left[\frac{i}{p^2 - m^2 + i\epsilon} - 2\pi n_F(p_0)\delta(p^2 - m^2) \right]_{m^2 \to 0} . \tag{A9}$$

Since only terms that contain a single δ function survive in the real part, we obtain, for (A6),

$$-2g^2 \int \frac{d^4 p}{(2\pi)^3} [1 - 2n_F(p_0)]\delta'(p^2)\frac{p_\mu k_\nu}{k^4} \langle\!\langle \tilde{G}_{\mu\beta}^a \tilde{G}_{\nu\beta}^a \rangle\!\rangle , \tag{A10}$$

where $\tilde{G}_{\mu\nu}^a$ is the dual tensor defined by $\frac{1}{2}\epsilon_{\mu\nu\lambda\rho}G_a^{\lambda\rho}$. Substituting $q_0 \to iq_0$, we obtain the results quoted in Eqs. (B2) and (B4).

The calculation of the diagrams in Fig. 1(d) is essentially the same as the one just described. The second term of Eq. (A7) does not contribute in this case and one gets the following result after some tedious but straightforward algebra:

$$-4g^2 \int \frac{d^4 p}{(2\pi)^3} [1 - 2n_F(p_0)]\frac{1}{k^2} \left[\frac{\delta(p^2)}{k^6} f_{\mu\nu}(p,k) - \frac{\delta'''(p^2)}{6} f_{\mu\nu}(k,p) \right] \langle\!\langle G_{\mu\beta}^a G_{\nu\beta}^a \rangle\!\rangle , \tag{A11}$$

with $f_{\mu\nu}(p,k) = (p \cdot k)k_\mu k_\nu - k^2 k_\mu p_\nu$. This can be shown to agree with (B3) and (B5). One should note that the above expressions can be obtained by simply substituting $1 \to 1 - 2n_F(p_0)$ in the zero-temperature result.

APPENDIX B

In this appendix we provide the full temperature dependence of the Wilson coefficients for reference. These coefficients were used in the calculation of the full curves in Figs. 6–11. We obtain the following expressions, which were obtained both in the imaginary-time and in the real-time formalism (see Appendix A)

$$\mathcal{C}_1 = \frac{1}{8\pi^2} \int_0^\infty \frac{dp_0^2}{p_0^2 + Q^2/4} \left\{ 1 + 4\frac{p_0^2}{Q^2} \left[1 - \tanh\left[\frac{p_0}{2T}\right] \right] \right\} , \tag{B1}$$

$$\mathcal{C}_{E^2}^{(a)} = -\frac{\alpha_s}{6\pi}\frac{1}{Q^4} - \frac{\alpha_s}{72\pi}\frac{1}{Q^2} \int_0^\infty dp_0^2 \left[1 - \tanh\left[\frac{p_0}{2T}\right] \right] \frac{p_0^2 - \frac{3}{4}Q^2}{(p_0^2 + Q^2/4)^3} , \tag{B2}$$

$$\mathcal{C}_{E^2}^{(b)} = -\frac{2\alpha_s}{9\pi}\frac{1}{Q^2} \int_0^\infty dp_0^2 \tanh\left[\frac{p_0}{2T}\right] \left[\frac{p_0^2 - \frac{3}{4}Q^2}{(p_0^2 + Q^2/4)^3} - \frac{1}{p_0^2(p_0^2 + Q^2/4)} \right] , \tag{B3}$$

$$\mathcal{C}_{B^2}^{(a)} = \frac{\alpha_s}{36\pi}\frac{1}{Q^2} \int_0^\infty dp_0^2 \left[1 - \tanh\left[\frac{p_0}{2T}\right] \right] \frac{p_0^2 - \frac{3}{4}Q^2}{(p_0^2 + Q^2/4)^3} , \tag{B4}$$

$$\mathcal{C}_{B^2}^{(b)} = -\frac{2\alpha_s}{9\pi}\frac{1}{Q^2} \int_0^\infty dp_0^2 \tanh\left[\frac{p_0}{2T}\right] \left[\frac{p_0^2 - \frac{3}{4}Q^2}{(p_0^2 + Q^2/4)^3} - \frac{1}{p_0^2(p_0^2 + Q^2/4)} \right] , \tag{B5}$$

$$\mathcal{C}_{(\bar{q}q)^2} = -\frac{112}{81}\pi\alpha_s . \tag{B6}$$

Note that we have performed one subtraction in (B1). Also, the coefficients $\mathcal{C}_{e^2}^{(b)}$ and $\mathcal{C}_{B^2}^{(b)}$ are infrared divergent at zero and finite temperature as discussed in the text.

---

[1]*Quark Matter '88*, proceedings of the 7th International Conference on Ultrarelativistic Nucleus-Nucleus Collisions, Lenox, Massachusetts, 1988, edited by G. Baym, P. Braun-Munzinger, and S. Nagamiya [Nucl. Phys. **A498** (1989)].

[2]J. Kogut, M. Stone, H. W. Wyld, S. Shenker, J. Shigemitsu, and D. K. Sinclair, Phys. Rev. Lett. **51**, 869 (1983).

[3]T. Celik, J. Engels, and H. Satz, Phys. Lett. **125B**, 411 (1983).

[4]A. I. Bochkarev and M. E. Shaposhnikov, Nucl. Phys. **B268**, 220 (1986).

[5]H. G. Dosch and S. Narison, Phys. Lett. B **203**, 155 (1988).

[6]R. J. Furnstahl, T. Hatsuda, and S. H. Lee, Phys. Rev. D **42**, 1744 (1990).

[7]M. A. Nowak, J. J. M. Verbaarschot, and I. Zahed, Nucl. Phys. **B324**, 1 (1989).

[8]M. A. Nowak, J. J. M. Verbaarschot, and I. Zahed, Nucl. Phys. **B325**, 581 (1989).

[9]A. A. Abrikosov, L. P. Gorkov, and I. E. Dzyaloshinski, *Methods of Quantum Field Theory in Statistical Physics* (Dover, New York, 1963).

[10]N. P. Landsman and Ch. G. van Weert, Phys. Rep. **145**, 141 (1987).

[11]K. G. Wilson, Phys. Rev. **129**, 1499 (1969).

[12]For a discussion of the validity of the OPE in the presence of condensates we refer to the original work, Ref. 13.

[13]M. A. Shifman, A. I. Vainshtein, and V. I. Zakharov, Nucl. Phys. **B147**, 385 (1979); **B147**, 448 (1979).

[14]H. Umezawa, H. Matsumoto, and M. Tachiki, *Thermo Field Dynamics and Condensed States* (North-Holland, Amsterdam,

1982).

[15]With our conventions, the energy density is given by $\Theta^{00} = :\Theta^{00}: + C(T)$, where $C(T)$ stands for the blackbody c-number contribution.

[16]E. S. Fradkin, Proc. P. N. Lebedev Phys. Inst. **29**, 3 (1965).

[17]M. S. Dubovikov and A. V. Smilga, Nucl. Phys. **B185**, 109 (1981).

[18]W. Hubschmid and S. Mallik, Nucl. Phys. **B207**, 29 (1982).

[19]V. A. Novikov, M. A. Shifman, A. I. Vainshtein, and V. I. Zakharov, Fortschr. Phys. **32**, 585 (1984).

[20]LHS and RHS always refer to the left-hand side or the right-hand side of Eq. (2.5).

[21]F. Karsch, Nucl. Phys. **B205** [FS5], 285 (1982).

[22]Y. Deng, in *Lattice '88,* proceedings of the International Symposiun, Batavia, Illinois, 1988, edited by A. S. Kronfeld and P. B. Mackenzie [Nucl. Phys. B (Proc. Suppl.) **9**, 334 (1989)].

[23]S. H. Lee, Phys. Rev. D **40**, 2484 (1989).

[24]J. B. Kogut and D. K. Sinclair, Phys. Rev. Lett. **60**, 1250 (1988).

[25]F. Karsch, J. B. Kogut, D. K. Sinclair, and H. W. Wyld, Phys. Lett. B **188**, 353 (1987).

[26]M. P. Grady, D. K. Sinclair, and J. B. Kogut, Phys. Lett. B **200**, 149 (1988).

[27]S. Gottlieb, W. Liu, R. L. Renken, R. L. Sugar, and D. Toussaint, Phys. Rev. D **41**, 622 (1990).

[28]O. Alvarez and R. D. Pisarski, Phys. Rev. D **26**, 3735 (1982).

[29]E. Manousakis and J. Polonyi, Phys. Rev. Lett. **58**, 847 (1987).

[30]It is known that the inclusion of radiative corrections to the perturbative calculation affects the theoretical predictions by about 5%.

[31]M. A. Shifman, A. I. Vainshtein, and V. I. Zakharov, Phys. Lett. **76B**, 471 (1978).

[32]J. J. Sakurai, *Currents and Mesons* (University of Chicago Press, Chicago, 1969).

[33]R. D. Pisarski, Phys. Lett. **110B**, 155 (1982).

[34]T. H. Hansson and I. Zahed, SUNY at Stony Brook report, 1990 (unpublished).